DOI: 10.1002/ ((please add manuscript number))

Article type: Communication

Polymer-passivated Inorganic Cesium Lead Mixed-halide Perovskites for Stable and Efficient Solar Cells with High Open-Circuit Voltage over 1.3 V

*Qingsen Zeng, Xiaoyu Zhang, Xiaolei Feng, Siyu Lu, Zhaolai Chen, Xue Yong, Simon A. T. Redfern, Haotong Wei, Haiyu Wang, Huaizhong Shen, Wei Zhang, Weitao Zheng, Hao Zhang, John S. Tse and Bai Yang**

Q. Zeng, Dr. X. Zhang, Dr. S. Lu, Dr. H. Shen, Prof. H. Zhang, Prof. B. Yang
State Key Laboratory of Supramolecular Structure and Materials, College of Chemistry, Jilin University, Changchun, 130012, P. R. China.
E-mail: byangchem@jlu.edu.cn
Dr. X. Zhang, Prof. W. Zhang, Prof. W. Zheng
Department of Materials Science, Key Laboratory of Mobile Materials MOE, State Key Laboratory of Automotive Simulation and Control, Jilin University, Changchun, 130012, China.
Dr. Z. Chen, Dr. H. Wei
Department of Mechanical and Materials Engineering, University of Nebraska-Lincoln, Lincoln, Nebraska 68588, USA.
X. Feng
State Key Laboratory of Superhard Materials, Jilin University, Changchun, 130012, C hina.
Dr. X. Yong, Prof. J.S. Tse
Department of Physics and Engineering Physics, University of Saskatchewan, Saskatoon, S7N5E2, Canada.
Prof. S. A. T. Redfern
Department of Earth Sciences, University of Cambridge, Downing Street, Cambirdge, CB2 3EQ, UK.
Prof. H. Wang
State Key Laboratory on Integrated Optoelectronics College of Electronic Science and Engineering, Jilin University, Changchun, 130012, P. R. China.

Abstract

Cesium-based trihalide perovskites have been demonstrated as promising light absorbers for photovoltaic applications due to its superb composition stability. However, the large energy losses (E_{loss}) in the conversion from photons to electrons observed in many inorganic perovskite solar cells has become a major hindrance impairing the ultimate efficiency of these devices. Here, we report an effective and reproducible method of modifying the interface between a $CsPbI_2Br$ absorber and polythiophene hole-acceptor to minimize the E_{loss}. We demonstrate that polythiophene, deposited on the top of $CsPbI_2Br$, can significantly reduce electron-hole recombination within the perovskite, which is due to the electronic passivation of surface defect states. In addition, the interfacial properties are improved by a simple annealing process, leading to significantly reduced energy disorder in polythiophene and enhanced hole-injection into the hole-acceptor. Consequently, one of the highest power conversion efficiency (PCE) of 12.02% from a reverse scan in stable inorganic mixed-halide perovskite solar cells is obtained under 100 mW cm^{-2} AM1.5G solar illumination. Modifying the perovskite films with annealing polythiophene enables an open-circuit voltage (V_{OC}) of up to 1.32 V, which is the highest value reported among cesium-lead mixed-halide perovskite solar cells. The E_{loss} of 0.5 eV is one of the lowest voltage deficits reported among inorganic perovskite photovoltaics to date. This method provides a new route to further improve the efficiency of perovskite solar cells by minimizing the E_{loss}.

Key words: polymer, inorganic perovskite, nanocrystals, solar cells, energy loss, surface passivation, defect states

Metal trihalide perovskites materials are promising for next-generation solution processed solar cells because of their high absorption coefficient,[1] long charge carrier recombination lifetime,[2-3] high charge carrier mobility,[4-6] and tunable bandgap.[7] As a result of rapid progress in both device architectures and compositional engineering, a certified power conversion efficiency (PCE) as high as 22.1% has been achieved.[8] The high efficiency of perovskite solar cells benefits from the high open-circuit voltage (V_{OC}) with low energy losses (E_{loss}).

The E_{loss} can be described by the equation: $E_{loss} = E_g - eV_{OC}$, where E_g is the optical-bandgap of the light absorber and e is the charge of an electron. Upon decreasing E_{loss}, V_{OC} will improve and thus the PCE will increase. An optimized organic-inorganic perovskite photovoltaic device generally has a high V_{OC} larger than 1 V with E_{loss} below 0.6 eV, which partially accounts for the high PCE of over 20%.[9-13] However, the thermally unstable nature of organic materials severely limits their commercial utility.[14] As an alternative, all-inorganic perovskites, prized for their superb stability toward moisture, light soaking and thermal stressing, have received a great deal of attention.[15-21] A variety of deposition techniques including spin coating,[22-28] two-step sequential method,[29-32] vapor deposition,[33-36] and spray-assisted deposition[37] have been developed to produce high-quality all-inorganic perovskite films. The recent achievement of strongly emissive $CsPbBr_3$ nanocrystal (NC) inks for photovoltaic prototype device has provided a new pathway for large-scale, single-step fabrication of perovskite solar cells.[22] In spite of rapid progress in film preparation, the efficiencies of all-inorganic perovskite solar cells

achieved to date leave much room for further improvement, principally as a result of their large E_{loss}.

Figure 1 shows plots of eV_{OC} against E_g for all inorganic perovskite solar cells reported so far, and the detail performance parameters are listed in **Table S1**. One of $CsPbI_3$ NC solar cell attains a PCE of 10.77% with the minimum E_{loss} of 0.52 eV.[23] The E_{loss} for most inorganic perovskite devices lies between 0.7 and 0.9 eV; for one of the $CsPbBr_3$ device, the value even reaches 1.06. Large values of E_{loss} reflect defect states,[38] energy disorder,[39] and/or inhomogeneous energy landscape[40] that generate nonradiative energy loss channels and thus lead to reductions in V_{OC}; hence there is considerable scope to increase the PCE of inorganic perovskite solar cells by boosting V_{OC}. Recently, the cesium lead mixed-halide perovskites, $CsPbI_2Br$, have attracted increasing attention, which is due to their better structure stability in the cubic phase than the fully iodide $CsPbI_3$ counterparts,[21,36] and reasonable broad bandgaps of 1.82 eV with great potential applying in semitransparent and tandem solar cells.[17] More recently, Park group reported efficient $CsPbI_2Br$ solar cells with the highest V_{OC} of 1.23 V by optimizing the crystallization process.[26] So far, the record efficiency of $CsPbI_2Br$ solar cells is around 11% with a V_{OC} of ~1.2 V. Therefore, it is of great urgent to reduce the E_{loss} to improve the V_{OC} and thus PCE of inorganic cesium lead mixed-halide perovskite solar cells.

In this paper, we report a systematic study to minimize the E_{loss} of $CsPbI_2Br$ perovskite solar cells. The photo-active layers are deposited from $CsPbI_2Br$ NC solution, and the as-prepared film exhibits a sharp band-tail that enables efficient

charge transfer, evidenced by the transient absorption (TA) spectra. Deep trap states can develop on perovskite crystals surface and induce strong charge recombination. We show here that electronic passivation of defect states can be achieved by depositing a thin poly(3-hexylthiophene) (P3HT) layer on the top of $CsPbI_2Br$ film, confirmed by theoretical calculations and photoluminescence (PL) spectra. In addition, the energy disorder in P3HT film was reduced after annealing, which dramatically enhanced hole-injection into the hole-acceptor simultaneously. The interfacial modification between the $CsPbI_2Br$ absorber and the P3HT hole-acceptor was found to improve the photovoltaic performance, and especially the V_{OC}, eventually resulting in a minimal E_{loss} of 0.50 eV (Figure 1). This led to one of the highest reported PCE of 12.02% from a reverse scan to date for inorganic mixed-halide perovskite solar cells (**Figure S1**). In addition, the optimal inorganic perovskite devices show excellent stability retain around 90% of their initial PCE after aging for near 1000 h.

We fabricated $CsPbI_2Br$ films by spin-coating with the corresponded NC solutions. Previously studies have shown that preparing Br-rich inorganic perovskite films using solution processing is difficult, which is due to solubility limitations of the CsBr precursor.[17,36] Here, we achieved high-quality $CsPbI_2Br$ perovskite films from their colloidal NCs for the first time. By using perovskite NCs we can precisely control the film thickness and composition. Energy disperse spectroscopy (EDS) measurements confirmed the Cs:Pb:I:Br elemental ratios of the as-prepared NCs to be 0.94:1.00:2.18:1.15, suggesting that the products can be considered as $CsPbI_2Br$ NCs (**Figure S2**). **Figure 2**a shows the optical absorption and PL spectra of $CsPbI_2Br$ NCs

in toluene. The absorption and PL peaks are located at 614 and 636 nm, respectively. Typical transmission electron microscopy (TEM) and high resolution TEM (HRTEM) images of purified $CsPbI_2Br$ NCs are given as insets in Figure 2a, showing the presence of rather monodisperse cubic-shaped NCs with an edge length of ~8.4 nm. The HRTEM highlights that $CsPbI_2Br$ NCs possess a well-defined crystalline structure with a cubic lattice parameter of 0.296 nm along the [100] direction.

The $CsPbI_2Br$ films were fabricated via a layer-by-layer (LBL) spin-coating method. In this method, a monolayer of NCs was deposited on a substrate by spin-coating and then soaked in $Pb(OAc)_2$ in anhydrous isopropanol (IPA) to remove the electrically-insulating ligands that originally solubilize the NCs. Smooth, crack-free perovskite films were readily produced by repeating this procedure until the desired film thickness was attained. The $CsPbI_2Br$ films were finally annealed at temperature of 265 ˚C to promote grain growth. The removal of insulating ligands leads to decrease in the NC spacing and triggers a Mott-type insulator-to-conductor transition that significantly affects the optical properties of the $CsPbI_2Br$ films.[41] As shown in Figure 2b, both the absorption and PL peaks gradually red-shift in the as-prepared, IPA washed, and annealed $CsPbI_2Br$ films. In the meantime, absorbance is enhanced across the whole spectrum. We ascribe the red-shift and the enhanced absorption to the increased crystal size and changes in effective dielectric constant at the surface of the crystals. Fourier-transform infrared (FTIR) spectra show that organic ligands are removed from the $CsPbI_2Br$ film after IPA washing (**Figure S3**) which leads to an increase in the dielectric constant of the surrounding medium, thus

enhancing the absorbance and contributing slightly to the red-shift.[42] Figure 2c, d, and e exhibit the surface morphology images of the three samples by scanning electron microscope (SEM), showing that the perovskite crystal size increases all the way from as-prepared to annealed films, which is responsible for the red-shift of absorption spectra. The annealed samples finally form smooth, compact $CsPbI_2Br$ films with an average grain size of 253 nm.

X-ray diffraction (XRD) patterns in Figure 2f provide information on the crystal structure of the three samples. As shown, $CsPbI_2Br$ film maintains the cubic phase even after IPA washing and high temperature annealing. The loss or weakening of some Bragg peaks indicates that the perovskite shows octahedral tilts and rotations as the ligands are removed and crystals grow.[43] Crystals within the annealed film are suggested to be highly oriented along the [100] and [110] direction. The gradual narrowing of the Bragg peaks is observed as the crystal size increases from SEM measurements. Time-resolved PL (TRPL) spectroscopy was carried out on these $CsPbI_2Br$ films. The results show that the PL lifetime tends to increase with increasing crystal size (Figure 2g, **Table S2**), which is similar to previous reports.[44]

Metallic Pb atoms can develop in perovskite and cause strong exciton quenching,[45] and the charge recombination centers are almost exclusively localized on the crystal surfaces rather than in the bulk.[38] During the ligands removal process, $CsPbI_2Br$ films were soaked in the $Pb(OAc)_2$ IPA solution. This results in Pb atom-rich perovskite films (**Figure S4**), and tends to have a high density of defect states. Optical characterization in Figure 2b confirms the existence of surface defects. As can be seen,

the Stokes shift increases from 18 nm in the as-prepared films to 35 nm in the annealed ones. Since the spontaneous radiative recombination between trap states causes a red-shift in the PL peak compared with that from the band edge transition,[46] the enhanced Stokes shift of the Pb-rich $CsPbI_2Br$ film here clearly demonstrates the appearance of surface defects.

Different passivating agents such as fullerene,[46] nitrogen-doped reduced graphene oxide,[47] the organic molecule iodopentafluorobenzene,[48] PbI_2,[49] thiophene, chlorine-capped TiO_2 colloidal NCs,[12] and pyridine Lewis bases[50] have been employed to passivate surface charge trap states of the perovskite. Here we find a simple but effective interface passivation method by using commercially available P3HT. A thin P3HT film coated on the top of $CsPbI_2Br$ film suppresses trap states and thus considerably reduces interface recombination at the $CsPbI_2Br$/P3HT interface. Steady-state PL and TRPL decay measurements were conducted to investigate the charge recombination occurring at the $CsPbI_2Br$/P3HT interface. An excitation light of 405 nm was used, which has a penetration depth of ~30 nm, much less than the thickness of $CsPbI_2Br$ films (200 nm). As shown in **Figure 3a**, the $CsPbI_2Br$ film without a P3HT layer had an emission peak at 664 nm, and was independent of the incident light directions. As expected, the $CsPbI_2Br$ layer passivated by P3HT (~5 nm) had a blue-shifted emission peak from 664 to 658 nm. The Stokes shift of $CsPbI_2Br$ decreased from 35 to 29 nm with the help of P3HT, indicating passivation of the surface trap states of the perovskite film.[46] TRPL spectroscopy was performed to evaluate the dynamics of charge carrier recombination in the perovskite film after

introducing P3HT. The film PL decay curves in Figure 3b also confirm the reduction of trap states. P3HT passivation causes the average lifetime of $CsPbI_2Br$ films increased from 6.91 to 14.8 ns (Table S2). Since the PL decay time of P3HT is well below 1 ns,[51] we consequently attribute the enhanced PL lifetime to the passivation of defect states.[52]

Electronic structure calculations based on the density functional theory (DFT) were performed to characterize how P3HT polymer can passivate the $CsPbI_2Br$ surface. First, the sulfur (S) atoms are found to bond with Cs atoms (Cs-S: 4.03 Å) on the $CsPbI_2Br$ (110) surface (Figure 3c) and passivate the interfacial positively charged under-coordinated Cs^+ ions. In addition, S atoms also boned to Pb (S-Pb: 3.36 Å) atoms and passivated the antisite defects (Figure 3d), known as deep-level defects and the most detrimental defects in perovskite solar cells.[53, 54] Without P3HT, the electron distribution was localized around the antisite defect site, which can capture charge carriers and induce charge recombination (Figure 3e). After P3HT coating, the electron distribution becomes delocalized, suggesting the localized states are passivated. In addition, the Cs-S and Pb-S bonds at the $CsPbI_2Br$/P3HT interface can be detected by the XPS measurements (**Figure S5**), confirming the results of calculations. In short, the introduction of P3HT results in a lower density of interfacial trap states, as well as strong binding between P3HT and perovskites.

Fast hole transfer from $CsPbI_2Br$ to P3HT happens after the film is annealed at 200 ˚C. The PL lifetimes of annealed $CsPbI_2Br$/P3HT films are shortened to 0.89 ns, which is much shorter than that of 1.85 ns for $CsPbI_2Br$/Spiro-OMeTAD films (Figure

3b, Table S2). The $CsPbI_2Br$ crystal size within the bilayer remained unchanged after annealing (**Figure S6**), indicating the decreased PL lifetime is not related to the change of grain size. In order to further investigate the hole transfer process, we studied the spectra distribution of photoexcited carriers in $CsPbI_2Br$/P3HT films using femtosecond broadband TA spectroscopy. The TA two-dimension color maps of the $CsPbI_2Br$/P3HT films before and after annealing are presented in **Figure 4a** and b. No redshift of the transient bleach peak is observed, indicating a flat energy landscape and negligible tail states below the bandgap.[40] This suggests that the $CsPbI_2Br$ films are promising for solar cells with minimized E_{loss}. On the other hand, the decay dynamics are much faster for the annealed bilayer films (Figure 4c), which is consistent with the TRPL results in Figure 3b. Half-lifetime for the annealed $CsPbI_2Br$/P3HT film decreases from over 1300 to ~400 ps, indicating annealed P3HT has efficient hole extraction in photovoltaic devices due to the good band alignments and strong interaction between $CsPbI_2Br$ and P3HT.

Energy disorder mitigation in charge transport layers has been demonstrated as a powerful method to reduce the E_{loss} of perovskite solar cells.[39] The annealing process is supposed to mitigate the energy disorder by reducing P3HT structural disorder.[39] The increased crystallinity of P3HT can be seen clearly in the XRD results shown in Figure 4d. The XRD patterns are obtained from a drop-cast P3HT film on top of the $CsPbI_2Br$. Increased intensity and narrowed peak width are observed in the Bragg peak at ~5˚, demonstrating improved crystallinity and indicating that a larger polymer crystal size is achieved.[55] Annealing may also influence the interface between the

P3HT and $CsPbI_2Br$. As shown in the inset of Figure 4d, the P3HT becomes soft during the annealing process, which effectively increases the contact area, thus the hole transfer paths. Overall, the annealing process promotes interface properties with lower interfacial energy disorder together with enhanced hole transfer from $CsPbI_2Br$ to P3HT, which are in good agreement with improved photovoltaic performance, especially improved V_{OC} with reduced E_{loss} (**Figure S7**, **Table S3**).

Figure 5a shows the schematics of the device structure and Figure 5b shows cross-sectional SEM image of the device. A thin layer of TiO_2 was employed as the electron-acceptor. We used ultraviolet photoelectron spectroscopy (UPS) to determine the band alignment at the P3HT/$CsPbI_2Br$ interface. UPS results of $CsPbI_2Br$ and P3HT are presented in **Figure S8**. The bandgaps of $CsPbI_2Br$ and P3HT are 1.82 (**Figure S9**b) and 1.9 eV,[56] respectively. Thus, we derived the valence band maximum (VBM) and the conduction band minimum (CBM) values for $CsPbI_2Br$ as -5.58 and -3.76 eV, respectively. Similarly, the highest occupied molecular orbital (HOMO) and lowest unoccupied molecular orbital (LUMO) energies for P3HT were estimated to be -4.94 and -3.04 eV. The band alignment demonstrates that P3HT acts as a hole-extraction/electron-blocking layer between the $CsPbI_2Br$ film and the anode (Figure 5c). The optimal energy level alignment will provide a driving force for the hole transfer and prevent electron from flowing in the opposite direction.

The best-performing $CsPbI_2Br$ solar cell completely fabricated and tested under ambient conditions exhibits a high PCE of 12.02% (Figure 5d). This is one of the highest efficiency among inorganic perovskite solar cells reported so far (Figure S1,

Table S1). The V_{OC} of the best-performing device is 1.30 V, which is the highest value among $CsPb(I/Br)_3$ solar cells. A high V_{OC}, as much as 1.32 V has also been achieved (Figure S7), corresponding to an E_{loss} of only 0.50 eV (Figure 1), demonstrating that the modification of interface with P3HT facilitates the charge extraction and transportation. The V_{OC} values of solar cells using annealed P3HT hole transport layers (HTLs) are almost 0.14 V higher than that of devices using spiro-OMeTAD-based HTLs, which further verifies the specific modification function of P3HT (Figure 5e). This is consistent with the smaller diode ideality factor (n) value of P3HT-based solar cells (**Figure S10**).[57] The photocurrents of our devices show a hysteresis under forward and reverse scanning directions (**Figure S11**), as has been reported previously for some inorganic perovskite planar heterojunction solar cells.[20, 36] Further modification of the cathode/perovskite interface will reduce the ionic defects in perovskites and thus eliminate the hysteresis phenomenon.[12, 58] An average PCE of 11.2% from 30 cells is achieved (Figure 5d, inset). We present the external quantum efficiency (EQE) between 300 and 750 nm in Figure S9a, and a band gap of 1.82 eV for the $CsPbI_2Br$ film is determined from the EQE spectrum (Figure S9b). A stabilized PCE of 9.50% and a stabilized J_{SC} of 9.60 mA cm^{-2} are achieved under the maximum power point output (**Figure S12**). In addition, the un-encapsulated polymer-modified devices exhibit great stability and retain around 90% of their initial PCE after 960 h of storage in a dry glovebox (Figure 5f). Noting that the modest improvements of V_{oc} and *FF* may be attributed to the more sufficient oxidation of P3HT, leading to enhanced p-doping of P3HT and thus the conductivity.[23] The

photo-stability under bias is also studied, and the light-induced aggravated halide segregation leads to device efficiency decrease (**Figure S13**).

In conclusion, in setting out to minimize the E_{loss} of inorganic $CsPbI_2Br$ solar cells, we performed a systematic study on the effects of modifying the interface between $CsPbI_2Br$ absorber and P3HT hole-acceptor. By passivating the surface defects of $CsPbI_2Br$, reducing the energy disorder of P3HT and increasing the contact area between $CsPbI_2Br$ and P3HT, we have significantly reduced the trap states, and facilitated the charge extraction and transportation, resulting in stable high-performance photovoltaic devices with high V_{OC} and low E_{loss} per absorbed photon. The important point is that our methods are simple and easy, and even without modifying the $CsPbI_2Br$ absorber layer. This work highlights the potential to achieve more efficient solar cells through careful optimization of interfaces between each layer.

Experimental Section

Synthesis of colloidal $CsPbI_2Br$ NCs: First, $CsPbI_3$ NCs and $CsPbBr_3$ NCs were synthesized using a reported procedure.[23] 0.75 g of Cs_2CO_3, 3 mL of OA and 75 mL of ODE were added to a 250 mL 3-necked round bottom flask. The reaction mixture was stirred under vacuum for about 2 h at 120 ℃. The reaction completed when the solution was clear, indicating that the Cs_2CO_3 has reacted with the OA. The Cs-oleate solution in ODE was stored in N_2 until it was needed for the NC synthesis. For the synthesis of $CsPbX(X=Br,I)_3$ NCs, 50 mL of ODE and 1g of PbI_2 or 0.8g of $PbBr_2$

were loaded into a 250 mL 3-necked flask, degassed and dried by applying vacuum for 1 h at 120 ℃. Dried OA (5 mL) and OLA (5 mL) were injected to the flask at this temperature. After the solution became clear, the temperature was raised to 180 ℃ and 8 mL of Cs-oleate (0.0625 M,preheated to 70 ℃) precursor was quickly injected. 10 sec later, the reaction mixture was cooled down to room temperature by an ice-water bath. The synthesized $CsPbX_3$ NCs were precipitated by adding 92 mL MeOAc (the ratio of NC reaction solution:MeOAc is 1:1.35) and then centrifuged at 8800 rpm for 10 min. Then the precipitate was redispersed in 12 mL of hexane and precipitated by adding 24 mL of MeOAc, and centrifuged again for 10 min at 8800 rpm. The $CsPbX_3$ NCs was redispersed in toluene at a concentration of ~50 mg/mL. $CsPbI_2Br$ NCs were synthesized via anion-exchange method following the previous report by Manna and Kovalenko.[59] Typically, 10 mL of dried ODE, 0.2 mL of dried OA and 0.2 mL of dried OLA were added into a 20 mL bottle. The reaction mixture was stirred under air atmosphere, and 124mg of $CsPbI_3$ NCs (0.172 mmol) and 50 mg of $CsPbBr_3$ NCs (0.086 mmol) were added into the bottle. 10 min later, the $CsPbI_2Br$ NCs were extracted via a similar procedure of $CsPbX_3$ NCs. Finally, the $CsPbI_2Br$ NCs were redispersed in toluene at a concentration of ~60 mg/mL and stored in freezer at 4 ℃ for device fabrication.

$CsPbI_2Br$ NC Film Deposition: The film was deposited similar to previous work with some improvement.[23] Ligand solutions were made by sonicating 30 mg of $Pb(OAc)_2$ in 30 mL of anhydrous IPA for 5 min. The solution was stored overnight to precipitate the excess salt. The $CsPbI_2Br$ NCs were spin-cast on the substrate at 600-800 RPM

for 20 sec followed by 2000 RPM for 5 sec, and then soaked in the ligand solution for removing the long-chain ligands. The film was rinsed using neat, anhydrous MeOAc, and then dried with a stream of air. This procedure was repeated multiple (2-5) times to build up 100 - 300 nm thick films.

Device Fabrication: The pre-patterned ITO was cleaned using chloroform, acetone, isopropanol and ethanol step by step before drying in a N_2 flow. Next, the ITO substrate was coated with the TiO_2 precursor at a speed of 2000 rpm. The TiO_2 precursors were prepared according to a previous work.[60] In brief, 4 mL tetrabutyl titanate (TBT) was dissolved in 2 mL IPA in a clean conical flask. 210 μL water and 17 μL concentrated HCl were mixed with 4 mL IPA, then this solution was dropped into the conical flask gradually, and the mixture was stirred for 12 h at room temperature. Before use, the resultant TiO_2 precursor was diluted with IPA. The TiO_2-coated ITO substrate was annealed at 450 ^oC for 20 min. The $CsPbI_2Br$ photoactive layer was deposited using the procedure described above, resulting in a total thickness of ~200 nm. The samples were put onto a hotplate at 265 ^oC. After cooling down to room temperature, the P3HT hole transporting material was spin-cast at 2500 rpm for 25 sec from a solution with a concentration of 15 mg of P3HT, 1 mL chlorobenzene, 54 μL of LiTFSI stock solution (10 mg/mL in acetonitrile), and 10.2 μL of TBP. The devices were annealed for 5 min at 200 ^oC, before 30 nm gold electrode was evaporated through a mask at pressure below 10^{-5} Torr. The overlap of the anode and cathode were the device areas to be 0.05 cm^{-2}. For the spiro-OMeTAD-based devices, operating conditions were similar to previous work.[10]

All of the processes were performed in air ambient at a relative humidity <15%.

Devices characterization: Devices were tested in air ambient. The solar simulators are Newport Oriel Sol3A solar simulators with xenon lamps. A calibrated Si reference solar cell was used to set the intensity of the lamp to 100 mW/cm^2 AM1.5 conditions. Current density-voltage (*J*-*V*) scans were taken from forward bias to reverse bias with a scan rate of 200 mV/s (scan parameters: step size = 20 mV, delay time = 10 ms). Devices were illuminated for 5 sec prior to starting the *J*-*V* sweep. To minimize possible J_{SC} overestimation from current collecting outside the device area, a mask was used, and the equivalent current densities was achieved for the solar cell. Stabilized power output was measured by holding the device at a constant voltage corresponding to the voltage at the maximum power point of the *J*-*V* scan. External quantum efficiency (EQE) spectra were recorded under illumination of monochromatic light from the halogen tungsten lamp using a monochromator (Enlitech, Taiwan) and detected by a computer-controlled lock-in amplifier. Please see some other characterizations in supporting information.

Supporting Information

Supporting Information is available from the Wiley Online Library or from the author.

Acknowledgements

Q. Zeng and X. Zhang contributed equally to this work. This work was financially supported by the National Science Foundation of China (NSFC) under Grant Nos. 51433003, the National Basic Research Program of China (973 Program) under Grant No. 2014CB643503, and the National Postdoctoral Program for Innovative Talents (BX201600060), and the JLU Science and Technology Innovative Research Team 2017TD-06.

Received: ((will be filled in by the editorial staff))
Revised: ((will be filled in by the editorial staff))
Published online: ((will be filled in by the editorial staff))

References

[1] C. Bao, Z. Chen, Y. Fang, H. Wei, Y. Deng, X. Xiao, L. Li, J. Huang, *Adv. Mater.* **2017**, *26*, 1703209.

[2] J. S. Manser, M. I. Saidaminov, J. A. Christians, O. M. Bakr, P. V. Kamat, *Acc. Chem. Res*. **2016**, *49*, 330.

[3] J.-W. Xiao, L. Liu, D. Zhang, N. D. Marco, J.-W. Lee, O. Lin, Q. Chen, Y. Yang, *Adv. Energy Mater.* **2017**, 7, 1700491.

[4] H. Wei, Y. Fang, P. Mulligan, W. Chuirazzi, H.-H. Fang, C. Wang, B. R. Ecker, Y. Gao, M.A. Loi, L. Cao, J. Huang, *Nat. Photon.* **2016**, *10*, 333.

[5] G. R. Yettapu, D. Talukdar, S. Sarkar, A. Swarnkar, A. Nag, P. Ghosh, P. Mandal, *Nano Lett.* **2016**, *16*, 4838.

[6] F. Li, H. Wang, D. Kufer, L. Liang, W. Yu, E. Alarousu, C. Ma, Y. Li, Z. Liu, C. Liu, N. Wei, F. Wang, L. Chen, O. F. Mohammed, A. Fratalocchi, X. Liu, G. Konstantatos, T. Wu, *Adv. Mater.* **2017**, *29*, 1602432.

[7] Y. Zhang, G. Grancini, Y. Feng, A. M. Asiri, M. K. Nazeeruddin, *ACS Energy Lett.* **2017**, *2*, 802.

[8] W. S. Yang, B.-W. Park, E. H. Jung, N. J. Jeon, Y. C. Kim, D. U. Lee, S. S. Shin, J. Seo, E. K. Kim, J. H. Noh, S. Il Seok, *Science*, **2017**, *356*, 1376.

[9] M. A. Haque, A. D. X. Guan, T. Wu, *Adv. Energy Mater.* **2017**, 7, 1602803.

[10] S. Yang, Y. Wang, P. Liu, Y.-B. Cheng, H. J. Zhao, H. G. Yang, *Nat. Energy*, 2016,

1, 15016.

[11] D. Bi, P. Gao, R. Scopelliti, E. Oveisi, J. Luo, M. Grätzel, A. Hagfeldt, M. K. Nazeeruddin, *Adv. Mater.* **2016**, *28*, 2910.

[12] H. Tan, A. Jain, O. Voznyy, X. Lan, F. P. García de Arquer, J. Z. Fan, R. Quintero-Bermudez, M. Yuan, B. Zhang, Y. Zhao, F. Fan, P. Li, L. N. Quan, Y. Zhao, Z.-H. Lu, Z. Yang, S. Hoogland, E. H. Sargent, *Science* **2017**, *355*, 722.

[13] P. Gratia, G. Grancini, J.-N. Audinot, X. Jeanbourquin, E. Mosconi, I. Zimmermann, D. Dowsett, Y. Lee, M. Grätzel, F. D. Angelis, K. Sivula, T. Wirtz, M. K. Nazeeruddin, *J. Am. Chem. Soc.* **2016**, *138*, 15821.

[14] B. Conings, J. Drijkoningen, N. Gauquelin, A. Babayigit, J. D'Haen, L. D'Olieslaeger, A. Ethirajan, J. Verbeeck, J. Manca, E. Mosconi, F. D. Angelis, H.-G. Boyen, *Adv. Energy Mater.* **2015**, *5*, 1500477.

[15] M. I. Saidaminov, M. A. Haque, J. Almutlaq, S. armah, X.-H. Miao, R. Begum, A. A. Zhumekenov, I. Dursun, N. Cho, B. Murali, O. F. Mohammed, T. Wu, O. M. Bakr, *Adv. Optical Mater.* **2017**, 5, 1600704.

[16] G. E. Eperon, G. M. Paterno, R. J. Sutton, A. Zampetti, A. A. Haghighirad, F. Cacialli, H. J. Snaith, *J. Mater. Chem. A* **2015**, *3*, 19688;

[17] R. E. Beal, D. J. Slotcavage, T. Leijtens, A. R. Bowring, R. A. Belisle, W. H. Nguyen, G. F. Burkhard, E. T. Hoke, M. D. McGehee, *J. Phys. Chem. Lett.* **2016**, *7*, 746;

[18] P. Luo, W. Xia, S. Zhou, L. Sun, J. Cheng, C. Xu, Y. Lu, *J. Phys. Chem. Lett.* **2016**, *7*, 3603;

[19] J. S. Niezgoda, B. J. Foley, A. Z. Chen, J. J. Choi, *ACS Energy Lett.* **2017**, *2*, 1043;

[20] J. K. Nam, S. U. Chai, W. Cha, Y. J. Choi, W. Kim, M. S. Jung, J. Kwon, D. Kim, J. H. Park, *Nano Lett.* **2017**, *17*, 2028.

[21] J.-F. Liao, H.-S. Rao, B.-X. Chen, D.-B. Kuang, C.-Y. Su, *J. Mater. Chem. A* **2017**, *5*, 2066.

[22] Q. A. Akkerman, M. Gandini, F. Di Stasio, P. Rastogi, F. Palazon, G. Bertoni, J. M. Ball, M. Prato, A. Petrozza, L. Manna, *Nat. Energy* **2016**, *2*, 16194.

[23] A. Swarnkar, A. R. Marshall, E. M. Sanehira, B. D. Chernomordik, D. T. Moore, J. A. Christians, T. Chakrabarti, J. M. Luther, *Science* **2016**, *354*, 92.

[24] T. S. Ripolles, K. Nishinaka, Y. Ogomi, Y. Miyata, S. Hayase, *Sol. Energy Mater. Sol. Cells* **2016**, 144, 532.

[25] W. Li, U. Rothmann, A. Liu, Z. Wang, Y. Zhang, A. R. Pascoe, J. Lu, L. Jiang, Y. Chen, F. Huang, Y. Peng, Q. Bao, J. Etheridge, U. Bach, Y.-B. Cheng, *Adv. Energy Mater.* **2017**, 7, 1700946

[26] J. K. Nam, M. S. Jung, S. U. Chai, Y. J. Choi, D. Kim, J. H. Park, *J. Phys. Chem. Lett.* **2017**, 8, 2936.

[27] W. Zhou, Y. Zhao, X. Zhou, R. Fu, Q. Li, Y. Zhao, K. Liu, D. Yu, Q. Zhao, *J. Phys. Chem. Lett.* **2017**, 8, 4122.

[28] C. F. J. Lau, M. Zhang, X. Deng, J. Zheng, J. Bing, Q. Ma, J. Kim, L. Hu, M. A. Green, S. Huang, A. Ho-Baillie, *ACS Energy Lett.* **2017**, *2*, 2319.

[29] M. Kulbak, D. Cahen, G. Hodes, *J. Phys. Chem. Lett.* **2015**, *6*, 2452;

[30] X. Chang, W. Li, L. Zhu, H. Liu, H. Geng, S. Xiang, J. Liu, H. Chen, *ACS Appl. Mater. Interfaces* **2016**, *8*, 33649;

[31] J. Liang, C. Wang, Y. Wang, Z. Xu, Z. Lu, Y. Ma, H. Zhu, Y. Hu, C. Xiao, X. Yi, G. Zhu, H. Lv, L. Ma, T. Chen, Z. Tie, Z. Jin, J. Liu, *J. Am. Chem. Soc.* **2016**, *138*, 15829;

[32] M. Kulbak, S. Gupta, N. Kedem, I. Levine, T. Bendikov, G. Hodes, D. Cahen, *J. Phys. Chem. Lett.* **2016**, *7*, 167.

[33] Q. Ma, S. Huang, X. Wen, M. A. Green, A. W. Y. Ho-Baillie, *Adv. Energy Mater.* **2016**, *6*, 1502202;

[34] C.-Y. Chen, H.-Y. Lin, K.-M. Chiang, W.-L. Tsai, Y.-C. Huang, C.-S. Tsao, H.-W. Lin, *Adv. Mater.* **2017**, *29*, 1605290;

[35] L. A. Frolova, D. V. Anokhin, A. A. Piryazev, S. Y. Luchkin, N. N. Dremova, K. J. Stevenson, P. A. Troshin, *J. Phys. Chem. Lett.* **2017**, *8*, 67.

[36] R. J. Sutton, G. E. Eperon, L. Miranda, E. S. Parrott, B. A. Kamino, J. B. Patel, M. T. Hörantner, M. B. Johnston, A. A. Haghighirad, D. T. Moore, H. J. Snaith, *Adv. Energy Mater.* **2016**, *6*, 1502458.

[37] C. F. J. Lau, X. Deng, Q. Ma, J. Zheng, J. S. Yun, M. A. Green, S. Huang, A. W. Y. Ho-Baillie, *ACS Energy Lett.* **2016**, 1, 573.

[38] R. J. Stewart, C. Grieco, A. V. Larsen, J. J. Maier, J. B. Asbury, *J. Phys. Chem. Lett.* **2016**, *7*, 1148.

[39] Y. Shao, Y. Yuan, J. Huang, *Nat. Energy* **2016**, *1*, 15001.

[40] M. Liu, O. Voznyy, R. Sabatini, F. P. Garcia de Arquer, R. Munir, A. H. Balawi,

X. Lan, F. Fan, G. Walters, A. R. Kirmani, S. Hoogland, F. Laquai, A. Amassian, E. H. Sargent, *Nat. Mater.* **2017**, *16*, 258.

[41] F. Remacle, *J. Phys. Chem. A* **2000**, *104*, 4739.

[42] J. Tang, L. Brzozowski, D. A. R. Barkhouse, X. Wang, R. Debnath, R. Wolowiec, E. Palmiano, L. Levina, A. G. Pattantyus-Abraham, D. Jamakosmanovic, E. H. Sargent, *ACS Nano* **2010**, *4*, 869.

[43] J. M. Luther, M. Law, Q. Song, C. L. Perkins, M. C. Beard, A. J. Nozik, *ACS Nano* **2008**, *2*, 271.

[44] V. Malgras, S. Tominaka, J. W. Ryan, J. Henzie, T. Takei, K. Ohara, Y. Yamauchi, *J. Am. Chem. Soc.* **2016**, *138*, 13874.

[45] H. Cho, S.-H. Jeong, M.-H. Park, Y.-H. Kim, C. Wolf, C.-L. Lee, J. H. Heo, A. Sadhanala, N. Myoung, S. Yoo, S. H. Im, R. H. Friend, T.-W. Lee, *Science* **2015**, *350*, 1222.

[46] Y. Shao, Z. Xiao, C. Bi, Y. Yuan, J. Huang, *Nat. Commun.* **2014**, *5*, 5784.

[47] M. Hadadian, J.-P. Correa-Baena, E. K. Goharshadi, A. Ummadisingu, J.-Y. Seo, J. Luo, S. Gholipour, S. M. Zakeeruddin, M. Saliba, A. Abate, M. Grätzel, A. Hagfeldt, *Adv. Mater.* **2016**, 28, 8681.

[48] A. Abate, M. Saliba, D. J. Hollman, S. D. Stranks, K. Wojciechowski, R. Avolio, G. Grancini, A. Petrozza, H. J. Snaith, *Nano Lett.* **2014**, 14, 3247.

[49] Q. Chen, H. Zhou, T.-B. Song, S. Luo, Z. Hong, H.-S. Duan, L. Dou, Y. Liu, Y. Yang, *Nano Lett.* **2014**, 14, 4158.

[50] N. K. Noel, A. Abate, S. D. Stranks, E. S. Parrott, V. M. Burlakov, A. Goriely, H.

J. Snaith, *ACS Nano* **2014**, 8, 9815.

[51] P. E. Shaw, A. Ruseckas, I. D. W. Samuel, *Adv. Mater.* **2008**, *20*, 3516.

[52] K. M. Sim, A. Swarnkar, A. Nag, D. S. Chung, Laser Photonics Rev. **2017**, *11*, 1700209.

[53] W.-J. Yin, T. Shi, Y. Yan, *Appl. Phys. Lett.* **2014**, *104*, 063903;

[54] A. Buin, P. Pietsch, J. Xu, O. Voznyy, A. H. Ip, R. Comin, E. H. Sargent, *Nano Lett.* **2014**, *14*, 6281.

[55] W. Ma, C. Yang, X. Gong, K. Lee, A. J. Heeger, *Adv. Funct. Mater.* **2005**, *15*, 1617.

[56] W. Zhang, R. Hu, D. Li, M.-M. Huo, X.-C. Ai, J.-P. Zhang, *J. Phys. Chem. C* **2012**, *116*, 4298.

[57] A. D. Sheikh, R. Munir, M. A. Haque, A. Bera, W. Hu, P. Shaikh, A. Amassian, T. Wu, *ACS Appl. Mater. Interfaces* **2017**, *9*, 35018.

[58] J.-P. Correa-Baena, A. Abate, M. Saliba, W. Tress, T. J. Jacobsson, M. Grätzel, A. Hagfeldt, *Energy Environ. Sci.* **2017**, DOI: 10.1039/c6ee03397k.

[59] G. Nedelcu, L. Protesescu, S. Yakunin, M. I. Bodnarchuk, M. J. Grotevent, M. V. Kovalenko, *Nano Lett.* **2015**, *15*, 5635.

[60] Q. Zeng, Z. Chen, F. Liu, G. Jin, X. Du, T. Ji, Y. Zhao, Y. Yue, H. Wang, D. Meng, T. Xie, H. Zhang, B. Yang, *Sol. RRL* **2017**, *1*, 1600020.

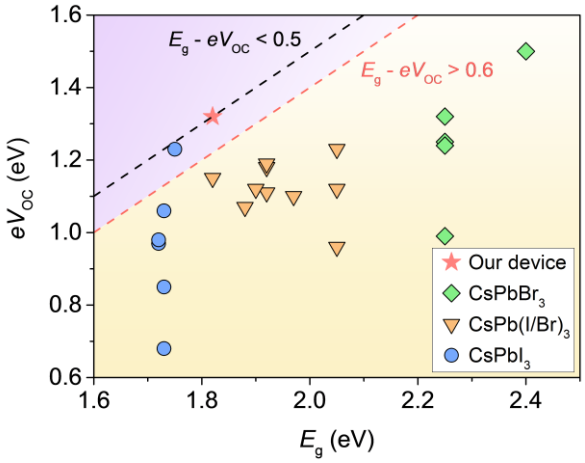

Figure 1. Plots of eV_{OC} against E_g for inorganic perovskite solar cells reported so far. Values of V_{OC} and E_g were taken from literatures. [16-20, 22-38]

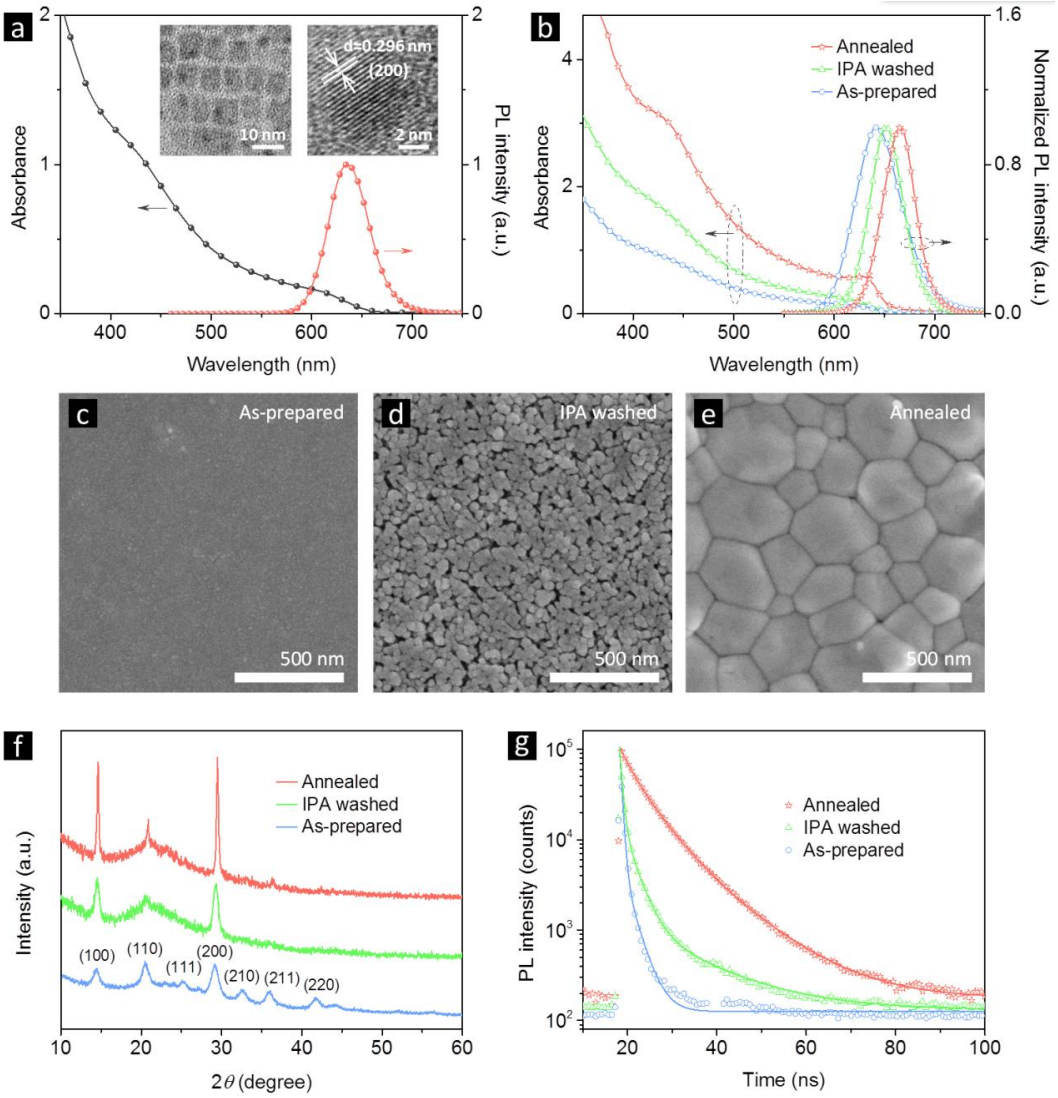

Figure 2. Characterization of solution-processed $CsPbI_2Br$ films deposited from colloidal NCs. (a) UV-visible absorption and steady-state PL spectra of $CsPbI_2Br$ NCs. Insets are TEM (left) and HRTEM (right) image of $CsPbI_2Br$ NCs. (b) UV-visible absorption and steady-state PL spectra of as-prepared, IPA washed and annealed $CsPbI_2Br$ films. SEM images of as-prepared (c), IPA washed (d) and annealed (e) $CsPbI_2Br$ films. (f) XRD patterns and (g) PL decay curves of as-prepared, IPA washed and annealed $CsPbI_2Br$ films.

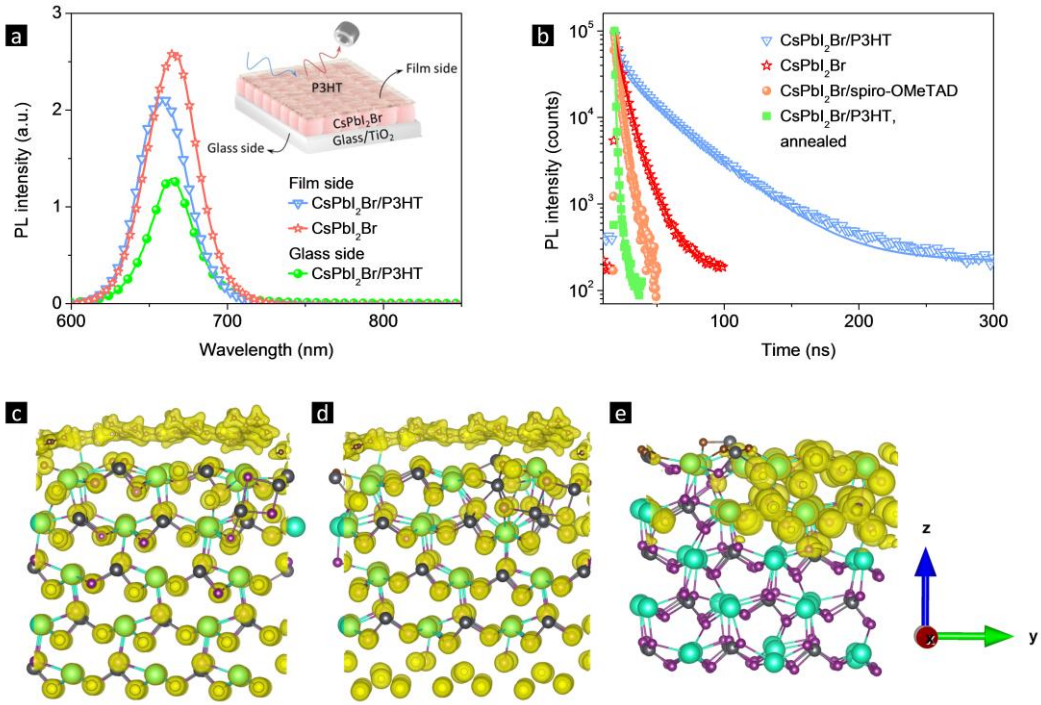

Figure 3. Surface trap state passivation with P3HT. (a) The steady-state PL spectra for $CsPbI_2Br$ films with P3HT layer using a 405 nm laser as the excitation source from the perovskite film side (blue curve), from the glass side (blue shadow), and $CsPbI_2Br$ films without P3HT from the perovskite film side (red curve). Inset shows the schematic of PL experiment set-up. Note that we chose a 405 nm laser as excitation source and a thin P3HT layer for this experiment in order to avoid the influence from PL of P3HT. (b) PL decay curves for $CsPbI_2Br$ film, the $CsPbI_2Br$/Spiro-OMeTAD film, the $CsPbI_2Br$/P3HT bilayer, and the annealed bilayer. The shorter decay time of the annealed $CsPbI_2Br$/P3HT bilayer than the $CsPbI_2Br$/spiro-OMeTAD film demonstrates the more efficient hole transfer from $CsPbI_2Br$ film due to the strong interaction between $CsPbI_2Br$ and P3HT. (c), (d), and (e) are density distribution plots of $CsPbI_2Br$ 110-surface. (c) P3HT on 110-surface, (d) P3HT on 110-surface with antisite defects, and (e) no P3HT on 110-surface with antisite defects.

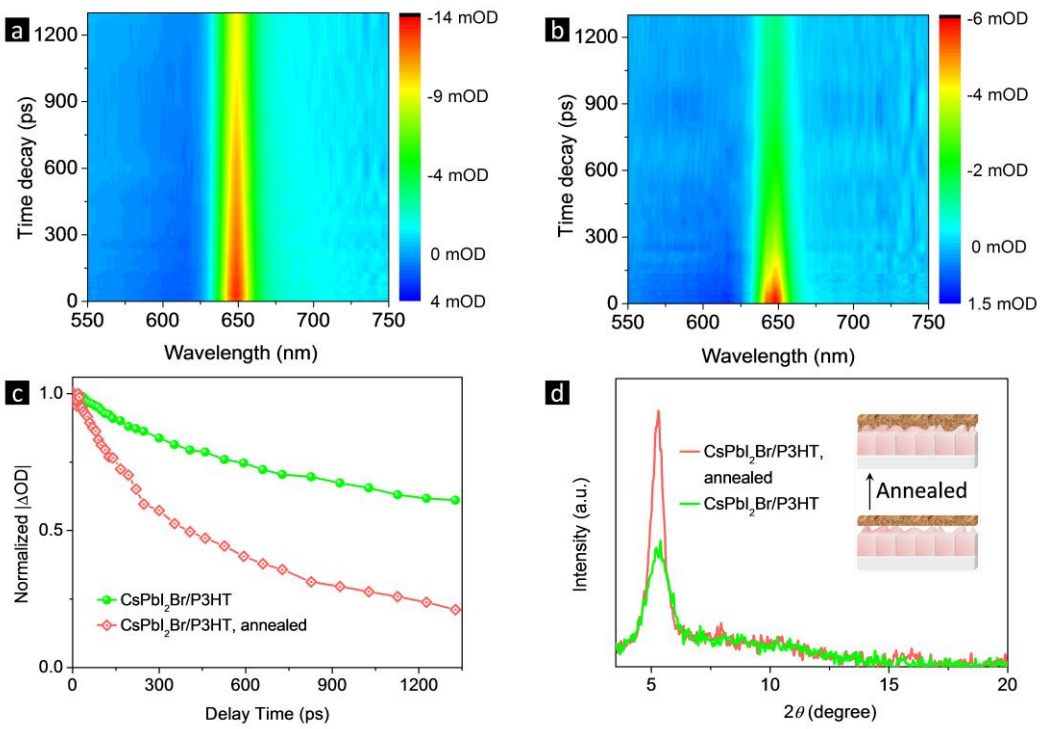

Figure 4. Enhanced interfacial properties by annealing. Spectro-temporal transient absorption maps for $CsPbI_2Br$/P3HT bilayers (a) before and (b) after annealing at 200 ^oC excited at 400 nm. (c) Characteristic dynamics for $CsPbI_2Br$/P3HT bilayers probed at 650 nm. (d) XRD patterns of P3HT films before and after annealing at 200 ^oC on $CsPbI_2Br$ substrates. The obvious narrowed peak width after annealing demonstrates the enlarged crystalline region. Inset presents schematic diagram of the evolution of perovskite and P3HT interface during annealing process.

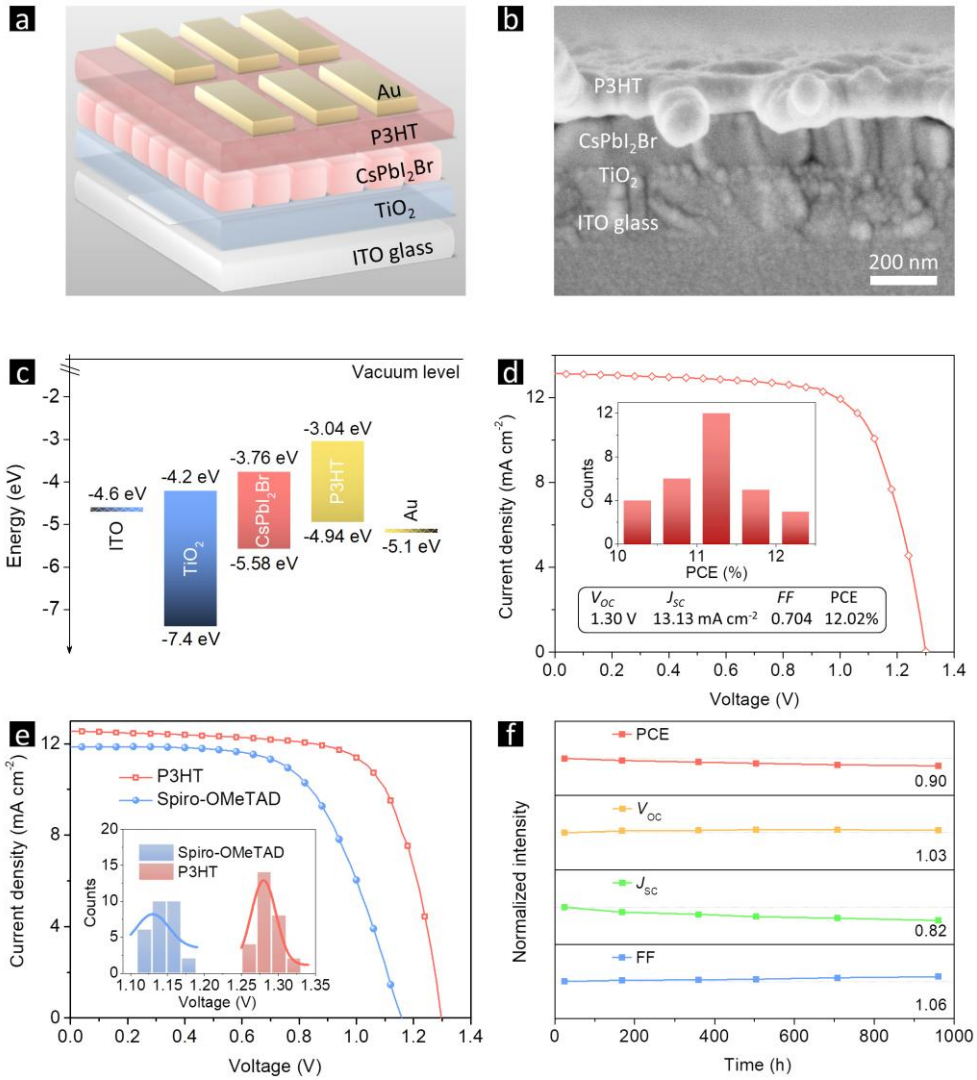

Figure 5. $CsPbI_2Br$ photovoltaic device structure and performance. (a) Device structure of our $CsPbI_2Br$ solar cells. (b) Cross-sectional SEM image of a $CsPbI_2Br$ device without Au electrode. (c) Schematic energy level diagram. The energy level of $CsPbI_2Br$ and P3HT was deduced from UPS results. (d) The reverse-scan current density-voltage (*J-V*) curves of the champion $CsPbI_2Br$ solar cell. The insets present the histogram of *J-V* scan efficiencies for 30 solar cells. The PCE was measured under 100 mW cm^{-2} AM 1.5G illumination, which has been corrected by a calibrated Si solar cell. (e) The reverse-scan *J-V* curves of the $CsPbI_2Br$ solar cells based on P3HT and frequently-used spiro-OMeTAD hole transport layers. Inset shows the histogram of V_{OC} for the $CsPbI_2Br$ solar cells using P3HT and spiro-OMeTAD hole transport layers. (f) Long-term PCE stability of a typical $CsPbI_2Br$ solar cell without encapsulations stored in a dried glovebox and tested once a week in open air with the relative humidity of ~15-40%.

The interfacial properties between $CsPbI_2Br$ absorber and P3HT hole-acceptor are improved by passivating the surface defects of $CsPbI_2Br$ and reducing the energy disorder of P3HT. Consequently, a stable inorganic perovskite solar cell with high PCE of 12.02% and minimal energy loss of 0.50 eV is obtained.

Keywords: polymer, inorganic perovskite, nanocrystals, solar cells, energy loss, surface passivation, defect states

Q. Zeng, Dr. X. Zhang, X. Feng, Dr. S. Lu, Dr. Z. Chen, Dr. X. Yong, Prof. S. A. T. Redfern, Dr. H. Wei, Prof. H. Wang, Dr. H. Shen, Prof. W. Zhang, Prof. W. Zheng, Prof. H. Zhang, Prof. J.S. Tse, Prof. B. Yang*

Polymer-passivated Inorganic Cesium Lead Mixed-halide Perovskites for Stable and Efficient Solar Cells with High Open-Circuit Voltage over 1.3 V

ToC figure